DALTON
FULL PAPER

Crystal structure of α-$Mg_2V_2O_7$ from synchrotron X-ray powder diffraction and characterization by ^{51}V MAS NMR spectroscopy

Ulla Gro Nielsen,[a] Hans J. Jakobsen,[a] Jørgen Skibsted *[a] and Poul Norby[b]

[a] *Instrument Centre for Solid-State NMR Spectroscopy, Department of Chemistry, University of Aarhus, DK-8000 Aarhus C, Denmark*
[b] *Department of Chemistry, University of Oslo, P.O. Box 1033, Blindern, N-0315 Oslo, Norway*

Received 21st May 2001, Accepted 24th August 2001
First published as an Advance Article on the web 12th October 2001

The crystal structure of the low-temperature form of magnesium pyrovanadate ($Mg_2V_2O_7$) has been determined from synchrotron X-ray powder diffraction data using Rietveld refinement. α-$Mg_2V_2O_7$ is isostructural with $Co_2V_2O_7$ and $Ni_2V_2O_7$. The Mg^{2+} ions are octahedrally coordinated to oxygen atoms in a distorted arrangement while the pyrovanadate anion has an approximately eclipsed conformation of non-bridging oxygen atoms. The ^{51}V MAS NMR spectra of the central and satellite transitions for the two distinct ^{51}V sites in α-$Mg_2V_2O_7$ allow determination of the magnitudes and relative orientations of the ^{51}V quadrupole coupling and chemical shift tensors. The crystal structure data are used to calculate the principal elements of the ^{51}V electric field gradient tensors employing the point-monopole approach. A good correlation between these elements and the experimental ^{51}V quadrupole tensor elements is observed, which allows assignment of the quadrupole coupling constants of C_Q = 4.80 MHz and C_Q = 3.33 MHz to the crystallographic V(1) and V(2) sites, respectively.

Introduction

Vanadium pentaoxide (V_2O_5) impregnated on a magnesium oxide (MgO) support can be used as a catalyst for oxidative dehydrogenation of hydrocarbons.[1–3] Similar catalytic reactions may be achieved using phases from the MgO–V_2O_5 system. For example, it has been shown that magnesium pyrovanadate is a catalyst for dehydrogenation of propane to propene[4] and that magnesium orthovanadate can be used for dehydrogenation of butane.[5] For both vanadates, it is believed that the catalytic activity and specificity are related to the structure of the VO_4 tetrahedra.

The most important and stable compounds in the MgO–V_2O_5 system are magnesium orthovanadate ($Mg_3(VO_4)_2$), the low- and high-temperature forms of the pyrovanadate (α- and β-$Mg_2V_2O_7$), and the metavanadate ($Mg(VO_3)_2$).[6] Crystal structures, determined from single-crystal X-ray diffraction, have been reported for these phases[7–9] with the exception of the low-temperature α-$Mg_2V_2O_7$ form. The lack of structural data for α-$Mg_2V_2O_7$ most likely reflects the fact that sufficiently large crystals for single-crystal XRD cannot be produced using high-temperature synthetic methods, because α-$Mg_2V_2O_7$ transforms into β-$Mg_2V_2O_7$ at 717 °C. Moreover, the corresponding β ⟶ α transition proceeds slowly at elevated temperatures and the β-form is stable at room temperature once formed.[6] Clark and Morley[6] found that the powder XRD pattern for α-$Mg_2V_2O_7$ closely resembles the pattern observed for $Co_2V_2O_7$ (monoclinic, $P2_1/c$).[10] Assuming α-$Mg_2V_2O_7$ to be isostructural with $Co_2V_2O_7$, they indexed the powder pattern for α-$Mg_2V_2O_7$ and reported the unit cell parameters. In this work we investigate α-$Mg_2V_2O_7$ by synchrotron X-ray powder diffraction and report a refinement of its crystal structure from these data. These structural parameters prove useful in the specific site assignment for the two ^{51}V resonances observed in the ^{51}V magic-angle spinning (MAS) NMR spectrum of α-$Mg_2V_2O_7$. Recently, we have investigated a series of ortho-, pyro-, and meta-vanadates by ^{51}V MAS NMR and determined the ^{51}V NMR parameters for the magnitudes and relative orientations of the ^{51}V quadrupole coupling and chemical shift anisotropy tensors.[11–14] These parameters reflect the local structure of the vanadium sites in a sensitive manner and allow differentiation of specific vanadium environments. For example, for the above-mentioned vanadates linear correlations are observed between the experimental quadrupole coupling tensor elements and the electric field gradient tensor elements obtained from point-monopole calculations.[12–14] Employing this approach and the refined structural data for α-$Mg_2V_2O_7$ an excellent correlation between the experimental and calculated ^{51}V quadrupole coupling tensor elements is obtained.

Experimental

The synthesis of α-$Mg_2V_2O_7$ was based on the method described by Sam *et al.*[4] 5.56 g (47.5 mmol) of NH_4VO_3 was dissolved in 50 mL of a 1% NH_3 solution and 4.75 g (47.4 mmol) of $Mg(OH)_2$ was added. The suspension was evaporated while being stirred and subsequently dried at 120 °C for two days. This precursor phase was calcined at 740 °C for 80 hours giving α-$Mg_2V_2O_7$ as confirmed by powder XRD.

Conventional X-ray powder diffraction data were collected on a Bruker D5000 powder diffractometer using Cu$K\alpha_1$-radiation from 10–90° in 2θ with a step size of 0.0154° in 2θ. Bragg–Brentano geometry was used with the sample deposited as a thin layer on a zero-background Si single-crystal sample holder. Synchrotron X-ray powder diffraction data were obtained at the Italian beamline (GILDA, BM8) at the European Synchrotron Radiation Facility (ESRF), Grenoble. The sample was contained in a 0.3 mm capillary. The detector used was a 25 × 40 cm FUJI imaging plate mounted on the Translating Imaging Plate (TIP) camera.[15–17] The data were read with a pixel size of 100 × 100 μm using a BAS2500 imaging plate scanner. The full plate was exposed and the data were extracted using FIT2D.[18] The wavelength (0.8267 Å) was determined from a LaB_6 (NIST SRM660) standard using FIT2D. Powder diffraction data for α-$Mg_2V_2O_7$ were collected from 7–45° in 2θ ($\sin\theta/\lambda_{max}$: 0.463).

Solid-state ^{51}V MAS NMR experiments were performed at 157.7 MHz (14.1 T) on a Varian INOVA-600 spectrometer using a home-built CP/MAS probe for 4 mm o.d. rotors. The

 DOI: 10.1039/b104454k

Table 1 Fractional atomic coordinates for α-$Mg_2V_2O_7$[a]

	x	*y*	*z*	U_{iso}(×100)[b]
Mg(1)	0.1481(4)	0.1214(4)	0.4635(3)	1.6(1)
Mg(2)	0.3121(5)	0.3895(4)	0.6821(3)	1.6(1)
V(1)	0.3591(2)	0.7587(2)	0.5400(2)	1.28(6)
V(2)	0.1919(2)	0.0199(2)	0.8151(2)	1.15(6)
O(1)	0.6108(8)	0.1282(5)	0.1224(5)	1.0(2)
O(2)	0.4310(8)	0.1307(5)	0.4010(5)	1.0(2)
O(3)	0.1713(7)	0.3698(6)	0.4592(5)	1.2(2)
O(4)	0.2507(8)	0.3580(5)	0.1881(6)	1.2(2)
O(5)	0.6773(8)	0.3728(7)	0.3510(6)	1.9(2)
O(6)	0.0254(7)	0.0769(5)	0.2454(5)	1.4(2)
O(7)	0.8503(7)	0.3783(5)	0.0028(5)	1.0(2)

[a] Space group: $P2_1/c$, a = 6.599(1) Å, b = 8.406(1) Å, c = 9.472(2) Å, β = 100.6085(4)°. Final agreement factors: R_P = 4.9%, R_{wP} = 6.9%, R_{F^2} = 4.2%. [b] Equivalent isotropic displacement parameter (Å^2).

^{51}V MAS NMR spectrum was recorded using a spinning speed ν_r = 15 kHz and a Varian rotor-speed controller, a spectral width of 2 MHz, single-pulse excitation with a pulse width of 0.5 μs ($\gamma B_1/2\pi \approx 55$ kHz), and a relaxation delay of 1 s. Exact magic-angle setting was achieved by minimizing the line widths of the spinning sidebands (ssbs) in the ^{23}Na MAS NMR spectrum of $NaNO_3$. Isotropic chemical shifts are relative to neat $VOCl_3$. Simulations, least-square optimizations, and error analyses of the experimental spectra were performed using the STARS software described elsewhere[19–21] and the same theoretical approach as recently employed in studies of ortho-, pyro-, and meta-vanadates.[12–14] It is noted that effects from non-uniform detection (*i.e.*, the quality factor (Q) of the probe circuitry)[19] have been included in the simulations, while the spectral distortions caused by non-uniform excitation are negligible as described elsewhere.[11,20] The quadrupole coupling parameters are defined as $C_Q = eQV_{zz}/h$ and $\eta_\sigma = (V_{yy} - V_{xx})/V_{zz}$. The anisotropic chemical shift parameters (δ_σ and η_σ) are defined by the principal elements of the chemical shift tensor as $\delta_\sigma = \delta_{iso} - \delta_{zz}$ and $\eta_\sigma = (\delta_{xx} - \delta_{yy})/\delta_\sigma$ where $\delta_{iso} = (\delta_{xx} + \delta_{yy} + \delta_{zz})/3$ and $|\delta_{zz} - \delta_{iso}| \geq |\delta_{xx} - \delta_{iso}| \geq |\delta_{yy} - \delta_{iso}|$. The Euler angles, defined in the ranges $0 \leq \psi \leq \pi$ and $0 \leq \chi, \xi \leq \pi/2$,[11] correspond to positive rotations about $\delta_{zz}(\psi)$, the new $\delta_{yy}(\chi)$ and the final $\delta_{zz}(\xi)$ axis.

Results and discussion

The conventional powder diffraction pattern of α-$Mg_2V_2O_7$ was indexed based on a monoclinic unit cell. The refined unit cell parameters (74 reflections) are: a = 6.599(1) Å, b = 8.406(1) Å, c = 9.472(2) Å, β = 100.6085(4)°, which are in good agreement with those reported by Clark and Morley.[6] Systematic extinctions are in accordance with the expected space group $P2_1/c$. Rietveld refinement of the synchrotron X-ray powder diffraction data was performed using the GSAS program suite.[22] Fractional coordinates reported for the structure of $Co_2V_2O_7$ were used as starting parameters for the Rietveld refinement. All atoms were refined with isotropic displacement parameters using X-ray scattering factors for V^{5+}, Mg^{2+} and O^-. The refinement converged with the agreement factors: R_P = 4.9%, R_{wP} = 6.9%, R_{F^2} = 4.2%. Refined unit cell parameters and atomic parameters from the final refinement cycle are given in Table 1 and the difference plot is shown in Fig. 1. Selected bond distances and angles are given in Table 2.

The refined structure reveals that α-$Mg_2V_2O_7$ contains octahedrally coordinated magnesium ions and isolated dimers of tetrahedrally coordinated vanadium ions as illustrated in Fig. 2. Octahedrally coordinated magnesium cations are linked together by pyrovanadate groups. An interesting and unusual feature in these pyrovanadates is the fact that the bridging oxygen in the pyrovanadate group (O(1)) is coordinated to a magnesium cation (Mg(1)). The V–O–V bond angle in the pyrovanadate group is therefore very small, 119.0(3)°. In addition, O(5) which is bonded to one vanadium (V(2)) is also coordinated to only one magnesium (Mg(2)) cation. The shortest V–O bond is between V(1) and O(5) and the V(1) site exhibits the largest variation in V–O bond lengths and O–V–O bond angles (*cf.* Table 2). Both magnesium atoms in α-$Mg_2V_2O_7$ have distorted octahedral coordination with mean Mg–O bond lengths of 2.086 Å and 2.107 Å for Mg(1) and Mg(2), respectively, and with the largest variation in Mg–O bond lengths and O–Mg–O bond angles observed for Mg(2) (*cf.* Table 2).

Table 2 Selected bond lengths (Å) and bond angles (°) for α-$Mg_2V_2O_7$

Mg(1)–O(2)	2.061(6)	Mg(2)–O(1)	2.153(6)
–O(3)	2.095(5)	–O(2)	2.084(5)
–O(4)	2.118(6)	–O(3)	2.151(5)
–O(6)	2.109(5)	–O(4)	2.122(5)
–O(7)	2.068(5)	–O(5)	2.025(5)
–O(7)	2.067(5)	–O(6)	2.106(5)
V(1)–O(1)	1.860(5)	V(2)–O(1)	1.820(5)
–O(2)	1.693(5)	–O(3)	1.676(5)
–O(5)	1.622(5)	–O(4)	1.681(5)
–O(7)	1.691(5)	–O(6)	1.656(4)
O(2)–Mg(1)–O(3)	83.3(2)	O(1)–Mg(2)–O(2)	93.5(2)
–O(4)	98.4(2)	–O(3)	89.3(2)
–O(6)	86.0(2)	–O(4)	97.3(2)
–O(7)	95.9(2)	–O(5)	88.2(2)
–O(7)	173.4(3)	–O(6)	176.0(2)
O(3)–Mg(1)–O(4)	85.8(2)	O(2)–Mg(2)–O(3)	170.3(2)
–O(6)	100.0(2)	–O(4)	86.1(2)
–O(7)	171.8(3)	–O(5)	102.6(2)
–O(7)	94.5(2)	–O(6)	85.5(2)
O(4)–Mg(1)–O(6)	173.1(3)	O(3)–Mg(2)–O(4)	84.3(2)
–O(7)	86.2(2)	–O(5)	86.8(2)
–O(7)	87.6(2)	–O(6)	92.4(2)
O(6)–Mg(1)–O(7)	88.1(2)	O(4)–Mg(2)–O(5)	169.5(3)
–O(7)	88.3(2)	–O(6)	86.5(2)
O(7)–Mg(1)–O(7)	87.2(2)	O(5)–Mg(2)–O(6)	88.3(2)
O(1)–V(1)–O(2)	115.1(2)	O(1)–V(2)–O(3)	105.9(2)
–O(5)	100.8(2)	–O(4)	113.9(2)
–O(7)	113.8(3)	–O(6)	107.4(3)
O(2)–V(1)–O(5)	109.1(3)	O(3)–V(2)–O(4)	108.0(2)
–O(7)	109.2(3)	–O(6)	111.0(2)
O(5)–V(1)–O(7)	108.4(3)	O(4)–V(2)–O(6)	110.6(2)
V(1)–O(1)–V(2)	119.0(3)		

The octahedrally coordinated magnesium cations form a three dimensional structure in α-$Mg_2V_2O_7$. This is quite different from the β-$Mg_2V_2O_7$ form, where the structure can be viewed as built from octahedra forming layers, which are connected by pyrovanadate anions. Also the conformation of the pyrovanadate group is different in the two structures as illustrated in Fig. 3. In α-$Mg_2V_2O_7$ the pyrovanadate group has an eclipsed conformation, while the conformation is staggered in the β-phase. For β-$Mg_2V_2O_7$ the vanadium cations form an additional weak fifth V–O bond (2.869 and 2.440 Å for V(1) and V(2), respectively).[8] The structure of β-$Mg_2V_2O_7$ is related to that of thortveitite,[23] but while thortveitite has a structure where the layers are comprised of edge-sharing octahedra, the layers in β-$Mg_2V_2O_7$ display edge- and corner-sharing. The high- and low-temperature structures of $Mg_2P_2O_7$[24,25] are strongly related to the thortveitite structure. However, the structure of α-$Mg_2V_2O_7$ is significantly different from these structures. The refined unit cell parameters and fractional atomic coordinates strongly resemble those determined for $Co_2V_2O_7$ and $Ni_2V_2O_7$,[10] demonstrating that α-$Mg_2V_2O_7$ can be considered isostructural with these pyrovanadates. Only small

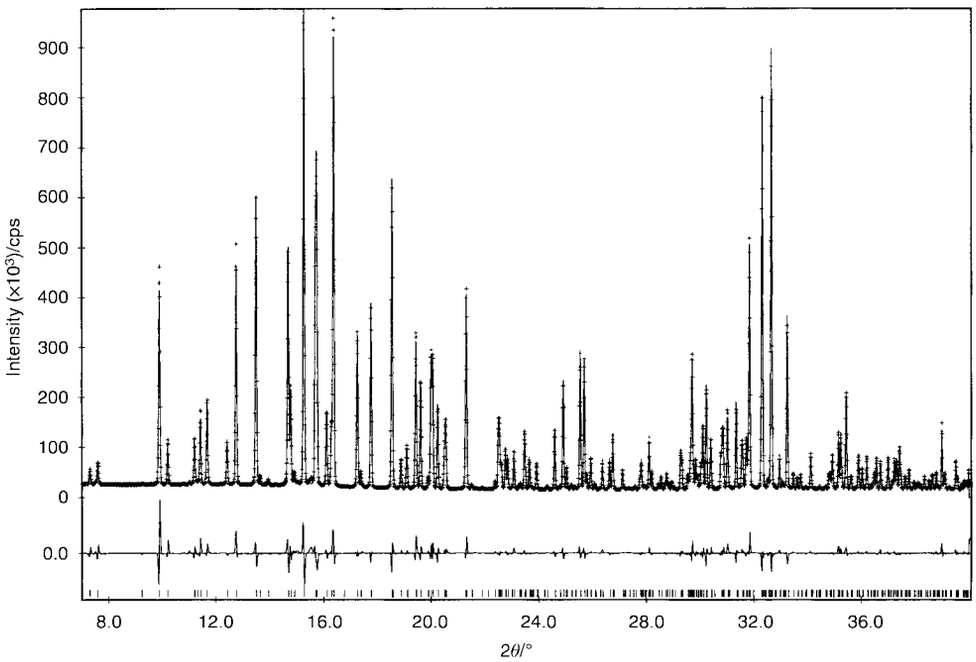

Fig. 1 Observed (+), calculated (——), and difference synchrotron X-ray powder diffraction patterns for α-$Mg_2V_2O_7$.

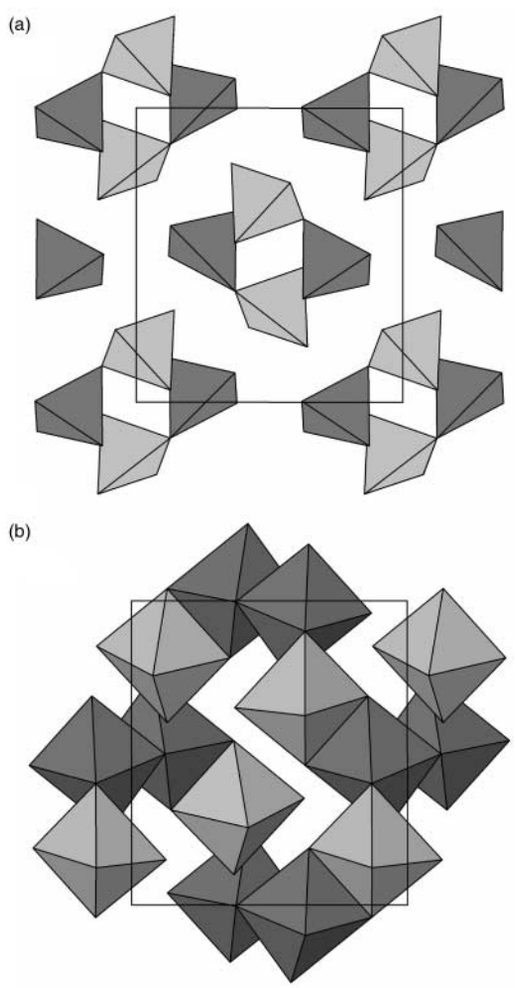

Fig. 2 Polyhedral representation for the structure of α-$Mg_2V_2O_7$ seen along the *a*-axis. Part (a) illustrates the pyrovanadate anions while part (b) shows the connectivity of the MgO_6 octahedra.

increases for the unit cell axes and the β angle are observed in going from $Ni_2V_2O_7$, $Co_2V_2O_7$ to α-$Mg_2V_2O_7$, while the V–O–V bond angle increases from 117.1° (117.6°) in $Ni_2V_2O_7$ ($Co_2V_2O_7$) to 119.0° in α-$Mg_2V_2O_7$.

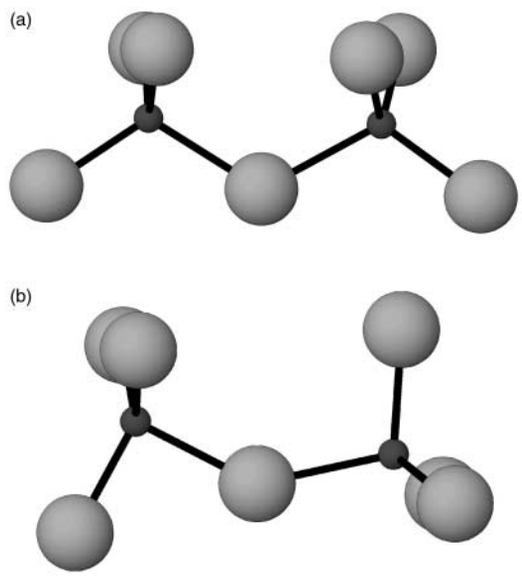

Fig. 3 Illustration for the conformation of the $V_2O_7^{4-}$ anion in (a) α-$Mg_2V_2O_7$ and (b) β-$Mg_2V_2O_7$. The plots employ the atomic coordinates in Table 1 for α-$Mg_2V_2O_7$ and those reported for β-$Mg_2V_2O_7$.[8]

The experimental ^{51}V MAS NMR spectrum of the central and satellite transitions for α-$Mg_2V_2O_7$, recorded at 14.1 T and for ν_r = 15.0 kHz, is illustrated in Fig. 4(a) and shows two well-separated manifolds of spinning sidebands (ssbs) from the two inequivalent vanadium atoms in α-$Mg_2V_2O_7$. The spectrum is dominated by the two isotropic peaks (right-hand inset in Fig. 4(a)) from the central transitions. This is a characteristic feature for vanadium environments influenced by a moderate chemical shift anisotropy (CSA). Furthermore, the ssbs for one of the manifolds exhibit partly resolved resonances from the individual satellite transitions (left-hand inset in Fig. 4(a)) as a result of a larger quadrupole coupling for this ^{51}V site leading to an observable difference in second-order quadrupolar shift for these transitions. Least-squares optimization of simulated to experimental ssb intensities, employing the approach described recently in the analysis of ^{51}V MAS NMR spectra of ortho-, pyro-, and meta-vanadates,[12–14] allows the determination of the ^{51}V NMR parameters for the quadrupole coupling

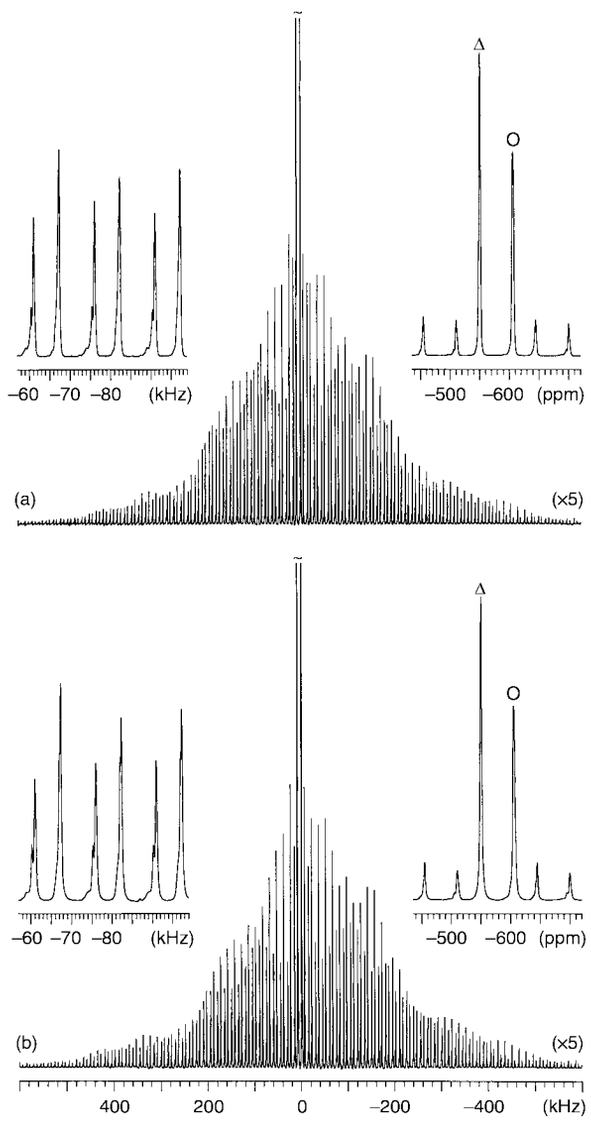

Fig. 4 (a) Experimental ^{51}V MAS NMR spectrum of α-$Mg_2V_2O_7$ recorded at 14.1 T (ν_L = 157.7 MHz) using a spinning speed ν_r = 15.0 kHz and illustrating the two manifolds of ssbs from the central and satellite transitions (kHz-scale relative to the midpoint of the two central transitions). The right-hand inset shows the spectral region for the isotropic peaks (on the ppm-scale), which are indicated by a circle and a triangle for V(1) and V(2), respectively. The left-hand inset illustrates that the ssbs for one of the manifolds (V(1)) exhibit partly resolved resonances as a result of the difference in second-order quadrupolar shifts for the individual satellite transitions. (b) Optimized simulation of the two overlapping manifolds of ssbs in (a) employing the ^{51}V NMR parameters in Table 3 and including second-order quadrupolar effects to account for the line shapes of the ssbs. An additional Gaussian line broadening of 350 Hz was employed in the simulation to give the best fit to the line widths observed in the experimental spectrum.

tensor (C_Q and η_Q), the chemical shift tensor, (δ_{iso}, δ_σ, η_σ) and the relative orientation of the two tensors (described by the Euler angles ψ, χ, and ξ). Employing this method and integrated ssb intensities for the two manifolds of ssbs gives the ^{51}V NMR parameters for the two vanadium sites in α-$Mg_2V_2O_7$ listed in Table 3. These data are employed in the optimized simulation (Fig. 4(b)) which reproduces all spectral features of the experimental spectrum, including the resolved second-order quadrupolar shifts observed for the satellite transitions for one of the ^{51}V sites. The CSA parameters for the two ^{51}V sites and the quadrupole coupling parameters for the site with the largest quadrupole coupling agree fairly well with those reported earlier by Occelli *et al.*[26] from ^{51}V MAS NMR spectra of the central transition at 7.1 and 11.7 T. However, our data should

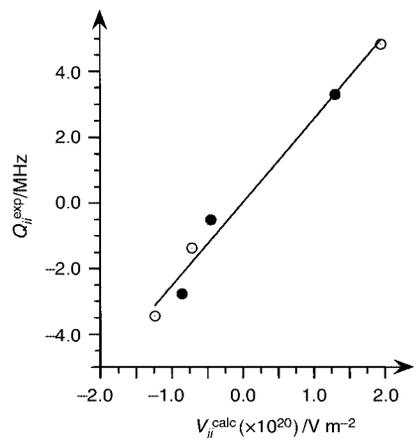

Fig. 5 Linear correlation between the ^{51}V quadrupole coupling tensor elements (Q_{ii}^{exp}) and calculated EFG tensor elements (V_{ii}^{calc}) from point-monopole calculations for the two V^{5+} sites in α-$Mg_2V_2O_7$. Open and filled circles correspond to the elements for the V(1) and V(2) sites, respectively.

be of higher precision because effects from both the quadrupole and CSA interactions are considered in the extraction of the parameters. ^{51}V CSA parameters have also been reported by Lapina *et al.*[27] These data differ significantly from those reported here and by Occelli *et al.*[26]

The ^{51}V NMR parameters in Table 3 may be assigned to the specific vanadium atoms in the refined crystal structure for α-$Mg_2V_2O_7$ from an estimation of the ^{51}V electric field gradients (EFGs) using point-monopole calculations.[12–14,28] This approach has recently proven very useful in the assignment of V^{5+} multiple sites in divalent metal pyro- and meta-vanadates.[13,14] The calculations include oxygen atoms only within the first coordination sphere of the V^{5+} ion and employ effective charges for the oxygens calculated from the bond-length bond-strength relations derived by Brown *et al.*[29,30] Employing this approach and the structural data from the synchrotron X-ray powder diffraction refinement (*i.e.*, Table 1) gives the following values for the principal elements of the ^{51}V EFG tensor ($\overline{V}$) for V(1): $V_{xx}^{calc} = -1.234$, $V_{yy}^{calc} = -0.715$, $V_{zz}^{calc} = 1.949$ and for V(2): $V_{xx}^{calc} = -0.854$, $V_{yy}^{calc} = -0.450$, $V_{zz}^{calc} = 1.304$, all numbers in units of 10^{20} V m^{-2}. These values may be correlated with the principal elements of the experimental quadrupole tensors ($\overline{Q}$) determined as:

$$Q_{zz}^{exp} = C_Q, \quad Q_{yy}^{exp} = -1/2(1 - \eta_Q)C_Q, \quad Q_{xx}^{exp} = -1/2(1 + \eta_Q)C_Q \quad (1)$$

and assuming positive values for C_Q, *i.e.* for the unique element of the EFG tensor (V_{zz}^{calc}). A plot of Q_{ii}^{exp} as a function of V_{ii}^{calc} is shown in Fig. 5 for the two ^{51}V sites in α-$Mg_2V_2O_7$ and demonstrates an excellent correlation between these parameters. Linear regression analysis of the data gives:

$$Q_{ii}^{exp} = 2.54\ V_{ii}^{calc}\ (10^{20}\ \text{V m}^{-2}) \quad (2)$$

with a correlation coefficient R = 0.990. Thus, this correlation allows assignment of the ^{51}V NMR parameters corresponding to the largest and the smallest quadrupole coupling to the V(1) and V(2) sites in α-$Mg_2V_2O_7$, respectively. The slope in eqn. (2) agrees well with the slope of 2.34 MHz/10^{20} V m^{-2} determined using the same model for a series of divalent metal pyro-vanadates.[14] Finally, we note that the assignment as given above can be obtained from point-monopole calculations employing the reported unit cell parameters from powder X-ray diffraction for α-$Mg_2V_2O_7$[6] and the fractional coordinates for either $Co_2V_2O_7$ or $Ni_2V_2O_7$.[10] However, such data result in less convincing correlations between Q_{ii}^{exp} and V_{ii}^{calc} compared to eqn. (2). This shows that the ^{51}V quadrupole coupling

Table 3 ^{51}V quadrupole coupling (C_Q, η_Q), chemical shift parameters (δ_σ, η_σ, δ_{iso}), and relative orientation (ψ, χ, ξ) of the two ^{51}V tensors for α-$Mg_2V_2O_7$ [a]

Site	C_Q/MHz	η_Q	δ_σ/ppm	η_σ	ψ /°	χ/°	ξ/°	δ_{iso}/ppm
V(1)	4.80 ± 0.08	0.42 ± 0.03	99 ± 5	0.55 ± 0.36	9 ± 45	85 ± 24	45 ± 19	−603.3 ± 0.5
V(2)	3.33 ± 0.05	0.67 ± 0.05	−58 ± 8	0.88 ± 0.20	106 ± 30	0 ± 14	15 ± 30	−549.1 ± 0.5

[a] For a definition of the ^{51}V NMR parameters, see the Experimental section.

parameters reflect the local environment of the vanadium atom in a very sensitive manner and that optimum relationships between ^{51}V NMR data and structural features require structural parameters of high precision.

Conclusions

The crystal structure of the low-temperature phase of magnesium pyrovanadate (α-$Mg_2V_2O_7$) has been refined from synchrotron X-ray powder diffraction data and found to be isostructural with $Co_2V_2O_7$ and $Ni_2V_2O_7$. The refined crystal structure data have allowed an assignment of the ^{51}V quadrupole coupling constants C_Q = 4.80 MHz and C_Q = 3.33 MHz (and thereby of the ^{51}V NMR parameters) to the V(1) and V(2) sites in α-$Mg_2V_2O_7$, respectively, from calculations of the ^{51}V electric field gradient tensors using the point-monopole approach. The convincing correlation between these elements and the experimental quadrupole tensor elements illustrates that precise structural parameters are required to obtain reliable correlations between ^{51}V NMR data and local structural features for V^{5+} sites in inorganic vanadates.

Acknowledgements

The use of the facilities at the Instrument Centre for Solid-State NMR Spectroscopy, University of Aarhus, sponsored by the Danish Natural Science Research Council, the Danish Technical Science Research Council, Teknologistyrelsen, Carlsbergfondet, and Direktør Ib Henriksens Fond, is acknowledged. J. S. thanks the Danish Natural Science Research Council for financial support (Grant No. 0001237).

References

1 E. A. Mamedov and V. C. Corberán, *Appl. Catal. A*, 1995, **127**, 1.
2 A. A. Lemonidou and A. E. Stambouli, *Appl. Catal. A*, 1998, **171**, 325.
3 A. A. Lemonidou, L. Nalbandian and I. A. Vasalos, *Catal. Today*, 2000, **61**, 333.
4 D. S. H. Sam, V. Soenen and J. C. Volta, *J. Catal.*, 1990, **123**, 417.
5 M. A. Chaar, D. Patel, M. C. Kung and H. H. Kung, *J. Catal.*, 1987, **105**, 483.
6 G. M. Clark and R. Morley, *J. Solid State Chem.*, 1976, **16**, 429.
7 N. Krishnamachari and C. Calvo, *Can. J. Chem.*, 1971, **49**, 1630.
8 R. Gopal and C. Calvo, *Acta Crystallogr., Sect. B*, 1974, **30**, 2491.
9 H. N. Ng and C. Calvo, *Can. J. Chem.*, 1972, **50**, 3619.
10 E. E. Sauerbrei, R. Faggiani and C. Calvo, *Acta Crystallogr., Sect. B*, 1974, **30**, 2907.
11 J. Skibsted, N. C. Nielsen, H. Bildsøe and H. J. Jakobsen, *J. Am. Chem. Soc.*, 1993, **115**, 7351.
12 J. Skibsted, C. J. H. Jacobsen and H. J. Jakobsen, *Inorg. Chem.*, 1998, **37**, 3083.
13 U. G. Nielsen, H. J. Jakobsen and J. Skibsted, *Inorg. Chem.*, 2000, **39**, 2135.
14 U. G. Nielsen, H. J. Jakobsen and J. Skibsted, *J. Phys. Chem. B*, 2001, **105**, 420.
15 P. Norby, *J. Appl. Crystallogr.*, 1997, **30**, 21.
16 P. Norby, *J. Am. Chem. Soc.*, 1997, **119**, 5215.
17 C. Meneghini, G. Artioli, P. Norby, A. Balerna, A Gualtieri and S. Mobilio, *J. Synchrotron Radiat.*, 2001, **8**, 1162.
18 A. P. Hammersley, S. O. Svensson and A. Thompson, *Nucl. Instrum. Methods Phys. Res., Sect. A*, 1994, **346**, 312.
19 J. Skibsted, N. C. Nielsen, H. Bildsøe and H. J. Jakobsen, *J. Magn. Reson.*, 1991, **95**, 88.
20 J. Skibsted, N. C. Nielsen, H. Bildsøe and H. J. Jakobsen, *Chem. Phys. Lett.*, 1992, **188**, 405.
21 J. Skibsted, T. Vosegaard, H. Bildsøe and H. J. Jakobsen, *J. Phys. Chem.*, 1996, **100**, 14872.
22 A. C. Larson and R. B. von Dreele, GSAS – General Structure Analysis System, 1994, Los Alamos National Laboratory Report LAUR 86–748, available by anonymous FTP from http://mist.lansce.lanl.gov
23 D. W. J. Cruickshank, H. Lynton and G. A. Barclay, *Acta Crystallogr.*, 1962, **15**, 491.
24 C. Calvo, *Acta Crystallogr.*, 1967, **23**, 289.
25 C. Calvo, *Can. J. Chem.*, 1965, **43**, 1139.
26 M. L. Occelli, R. S. Maxwell and H. Eckert, *J. Catal.*, 1992, **137**, 36.
27 O. B. Lapina, V. M. Mastikhin, A. A. Shubin, V. N. Krasilnikov and K. I. Zamareaev, *Prog. Nucl. Magn. Reson. Spectrosc.*, 1992, **24**, 457.
28 H. Koller, G. Engelhardt, A. P. M. Kentgens and J. Sauer, *J. Phys. Chem.*, 1994, **98**, 1544.
29 I. D. Brown and R. D. Shannon, *Acta Crystallogr., Sect. A*, 1973, **29**, 266.
30 I. D. Brown and D. Altermatt, *Acta Crystallogr., Sect. B*, 1985, **41**, 244.